Highlights

Qualitative study of ballistic capture at Mars via Lagrangian descriptors

A. Quinci, G. Merisio, F. Topputo

- Lagrangian descriptors highlight regions with different dynamical behavior.

- Geometrical singularities are extracted with Roberts' edge detection method.

- Dynamics separatrices are inspected against the weak stability boundary.

- Insight about the ballistic capture problem in the proximity of Mars is provided.

- Lagrangian descriptors are convenient for designing ballistic capture orbits.

Qualitative study of ballistic capture at Mars via Lagrangian descriptors

Alessio Quinci[a,*], Gianmario Merisio[a,**] and Francesco Topputo[a]

[a]*Department of Aerospace Science and Technology, Politecnico di Milano, Via La Masa 34, Milano 20156, Italy*

ARTICLE INFO

ABSTRACT

Lagrangian descriptors reveal the dynamical skeleton governing transport mechanisms of a generic flow. In doing so, they unveil geometrical structures in the phase space that separate regions with different qualitative behavior. This work investigates to what extent Lagrangian descriptors provide information about non-Keplerian motion in Mars proximity, which is modeled under the planar elliptic restricted three-body problem. We propose a novel technique to reveal ballistic capture orbits extracting separatrices of the phase space highlighted by Lagrangian descriptor scalar fields. The Roberts' operator to approximate the gradient is used to detect the edges in the fields. Results demonstrate the chaos indicator ability to distinguish sets of initial conditions exhibiting different dynamics, including ballistic capture ones. Separatrices are validated against reference weak stability boundary derived on similar integration intervals. Compared to other techniques, Lagrangian descriptors provide dynamics insight bypassing the propagation of the variational equations.

1. Introduction

Ballistic capture (BC) orbits are low-energy transfers that allow temporary capture about a planet exploiting the natural dynamics, thus without requiring maneuvers [33]. Compared to Keplerian solutions, they are cheaper and more versatile from the operational perspective at the expense of longer transfer times. BC orbits are bounded by the weak stability boundary (WSB) [3, 6, 11, 33]. After being initially conceived as a fuzzy boundary region in the Sun–Earth–Moon system [1, 5], the WSB was algorithmically defined in [2]. The definition was later extended in [15, 31, 32]. A formal definition and a technique for its derivation were proposed in [19].

Approaches currently known for designing BC orbits are: i) the technique stemmed from invariant manifolds [4, 13, 34], ii) the method based on stable sets manipulation [19, 22, 23, 32], iii) the Hamiltonian approach taking advantage of canonical transformations [10], and iv) the multiple shooting technique to solve a sequence of three-point boundary value problems [26]. The first methodology gives insights into the dynamics but it is only applicable to autonomous systems (e. g., the circular restricted three-body problem), while the others can be applied to more representative, non-autonomous models. Lately, the variational theory for Lagrangian coherent structures (LCSs) [17, 18], and the Taylor differential algebra [37] were applied to derive BC orbits and the WSB more efficiently [8, 25, 35]. Alternatively, Lagrangian descriptors (LDs) can be exploited. They reveal separatrices, so providing a qualitative description of the dynamics and highlighting the geometrical template of phase space structures even for systems with generic time dependence [7, 20, 21, 24, 28].

The goal of the paper is to study to what extent LDs inform about the BC mechanism and aid in the design of BC orbits. We provide a characterization of the dynamics in the Mars proximity modeled under the planar elliptic restricted three-body problem (ER3BP). The geometrical structures featured by LD scalar fields are extracted through an edge detection algorithm based on the Roberts' method [14]. Specifically, Roberts' operator is used to approximate the gradient of the field [30]. The separatrices are inspected against the WSB derived on similar integration intervals. For a coherent comparison, the particle stability definition is modified to relax the geometrical constraint on the number of completed revolutions [19, 23]. Results show a strong correlation between extracted separatrices and the WSB,

---

*Corresponding author
**Principal corresponding author
✉ alessio.quinci@mail.polimi.it (A. Quinci); gianmario.merisio@polimi.it (G. Merisio);
francesco.topputo@polimi.it (F. Topputo)
ORCID(s): 0000-0002-7792-4581 (A. Quinci); 0000-0001-8806-7952 (G. Merisio); 0000-0002-5369-6887 (F. Topputo)

Table 1
Sun–Mars physical parameters.

Parameter	Unit	Value	Description	Reference
μ	-	$3.226\,201 \times 10^{-7}$	Mass parameter	
a_p	AU	$1.523\,688$	Primaries semi-major axis	[19]
e_p	-	$0.093\,418$	Primaries eccentricity	
R	km	3397	Mars mean equatorial radius	
R_{SOI}	km	$170R$	Mars sphere of influence (SOI) radius	[23]

particularly when the geometrical structures governing the transport mechanisms emerge. Eventually, capture sets at Mars are identified in the intricate plot of separatrices.

The remainder of the paper is organized as follows. In Section 2, the dynamical model is described. The methodology is discussed in Section 3. Results are shown in Section 4. Eventually, conclusions are drawn in Section 5.

2. Equations of motion

The planar ER3BP describes the motion of a massless particle moving under the gravitational attraction of two primary bodies P_1 (the Sun) and P_2 (Mars) without influencing their motion. The two primaries revolve on ellipses about their common barycenter, influenced only by their mutual attraction. The model is expressed in the synodic reference frame centered at the primaries barycenter. The synodic frame non-uniformly rotates and pulsates to keep their distance equal to one [19]. Let the mass parameter $\mu = m_2/(m_1 + m_2)$, where m_1 and m_2 are the masses of P_1 and P_2, respectively. The positions of P_1 and P_2 are (-μ, 0) and (1-μ, 0), respectively. The equations of motion (EoM) are scaled such that the sum of P_1 and P_2 masses is set to one as well as their distance, and their period is scaled to 2π [19]. The true anomaly f is designated as the independent variable of the system. The EoM read [19]

$$x'' - 2y' = \omega_x$$
$$y'' + 2x' = \omega_y \tag{1}$$

where primes represent differentiation with respect to the true anomaly f that depends on the scaled time as [19]

$$\frac{\mathrm{d}f}{\mathrm{d}t} = \frac{(1 + e_p \cos f)^2}{(1 - e_p^2)^{3/2}}. \tag{2}$$

In Eq. (1), subscripts $(\cdot)_x$ and $(\cdot)_y$ denote the partial derivatives of the potential function ω defined as [19]

$$\omega(x, y, f) = \frac{1}{1 + e_p \cos f} \left[\frac{1}{2}\left(x^2 + y^2\right) + \frac{1 - \mu}{r_1} + \frac{\mu}{r_2} + \frac{1}{2}\mu(1 - \mu) \right], \tag{3}$$

with $r_1 = \sqrt{(x + \mu)^2 + y^2}$ and $r_2 = \sqrt{(x + \mu - 1)^2 + y^2}$ the distances of the particle from P_1 and P_2, respectively, while e_p is the common eccentricity of the primaries. The Sun–Mars physical parameters used in this study are reported in Table 1. The EoM are integrated with a 8th-order Runge–Kutta scheme with a 7th-order embedded step-size control. The integration relative tolerance is set to 10^{-9} [27, 36].

3. Methodology

3.1. Low-energy regime

BC orbits can be identified as those solutions allowing for material transfer between interior and exterior realms [12]. In the circular restricted three-body problem (CR3BP), they could be quantitatively identified as trajectories with Jacobi constant just below that of the collinear Lagrangian points L_1 and L_2. In the Sun–Mars system under study, this means trajectories with $C_J < C_{J1} = 3.000\,203$ (i. e., transfers between primary and secondary interior realms) and $C_J < C_{J2} = 3.000\,202$ (i. e., transfers between interior and exterior realms) [12]. On the other hand, when the Jacobi constant falls below that of the collinear Lagrangian point L_3 ($C_J < C_{J3} = 3.000\,001$), then high-energy transfers are found [9, 29]. However, qualitative statement on allowed and forbidden regions are no longer possible in the elliptic problem since the Jacobi value becomes anomaly-dependent [19].

3.2. Particle stability definition

Particle stability is inferred using an alternative formulation of the stable sets defined in [23]. While propagating initial conditions (ICs) in the non-dimensional, synodic reference frame, the particle non-dimensional distance $r(f)$ and Kepler energy $H(f)$ with respect to the target body P_2 are computed [19]. The following indications are used to classify stability: A) a particle escapes at $f = f_e$ if $H(f_e) > 0 \land r(f_e) > R_{SOI}$; B) a particle impacts the surface of the target at $f = f_i$ if $r(f_i) < R$. Based on its dynamical behavior over the integration interval $[f_0, f_f]$, a propagated trajectory is said to be: i) *weakly stable* if the particle neither escape nor impact with the target, so belonging to the subset $\mathcal{W}(f_f)$; ii) *unstable* if the particle escapes from the target before f_f, then condition A) is verified for $f_e \in [f_0, f_f]$, so belonging to the subset $\mathcal{X}(f_f)$; iii) *crash* if the particle impacts with the target before f_f, then condition B) is verified for $f_i \in [f_0, f_f]$, so belonging to the subset $\mathcal{K}(f_f)$. A capture set is defined as $\mathcal{C}(f_B, f_F) := \mathcal{X}(f_B) \cap \mathcal{W}(f_F)$ where $f_B < f_0$ (backward leg), and $f_F > f_0$ (forward leg).

If neither the escape criteria nor the impact criteria are matched, then the orbit is considered weakly stable in the interval $[f_0, f_f]$, independently of the type of orbit considered. The definition adopted in this study is the same used in [19, 23]. The aforementioned alternative particle stability formulation only regards the count of revolutions about the target, which in this work is neglected.

3.3. Lagrangian descriptors

By manipulating the definition given in [24], we define the LD as

$$M(\mathbf{x}_0, f_0, f_B, f_F) = \int_{f_0+f_B}^{f_0} |\mathcal{F}(\mathbf{x}(f))|^\gamma \mathrm{d}f + \int_{f_0}^{f_0+f_F} |\mathcal{F}(\mathbf{x}(f))|^\gamma \mathrm{d}f, \tag{4}$$

where $\mathbf{x} = [x, y, x', y']$ is the state vector obtained by rearranging Eq. (1) as a four-dimensional, first-order system of ordinary differential equations $\mathbf{x}' = \mathbf{f}(\mathbf{x}, f)$. The integrand $|\mathcal{F}(\mathbf{x}(f))|^\gamma$ in Eq. (4) is a bounded, positive quantity, while γ is the exponent defining the norm [24]. In this study, we select $\mathcal{F} := \sqrt{(x')^2 + (y')^2}$ and $\gamma = 1/2$ because they highlight the geometrical structures of the phase space better than the other integrands and norms as in [24]. The LD field is then defined as $\mathcal{M}(f_0, f_B, f_F) := \{M(\mathbf{x}_0, f_0, f_B, f_F) \mid \mathbf{x}_0 \in \Omega\}$, where Ω is the set containing the ICs. In practise, the LD is computed appending its integrand to the space state equations with a zero initial value, and propagating the extended dynamics. The integration of the extended dynamics is stopped at f_i if the particle impacts with the target body.

An abrupt change in the LD field yelds discontinuous derivatives along the direction transverse to the change. Such singularities coincide with phase space structures separating trajectories with different dynamics, so abrupt changes correspond to dynamics separatrices [24]. In Eq. (4), $M(\mathbf{x}_0, f_0, 0, f_F)$ isolates dynamics separatrices obtained propagating ICs forwards, thus they are linked to repelling LCSs. Conversely, $M(\mathbf{x}_0, f_0, f_B, 0)$ reveals separatrices backwards, so highlighting the attracting LCSs [21].

3.4. Extraction of separatrices

The structures revealed by the LD field are extracted with an edge detection algorithm. Edge detection is an image processing technique usually exploited for finding boundaries of objects within images. An edge is defined as the locus of points where an abrupt change in intensity of the image occurs. Several edge detection algorithms are available (e. g., Sobel, Prewitt, Roberts, Canny, and zero-cross methods) [14]. Roberts' operator appears to be the most effective in extracting edges from the LD field of the problem at hand [30].

Given the image of the scalar field, the algorithm finds edges at those points where the gradient magnitude of the image is larger than a sensitivity threshold σ provided as input. The gradient of the image is approximated by computing the sum of the squares of the differences between diagonal neighbors pixels [14, 30]. The threshold value is tuned[1] to show as many structures as possible associated to abrupt changes in the LD field.

3.5. Validation of separatrices

The dynamics separatrices extracted from the LD field are expected to match the WSB computed on the same integration interval. The validation procedure devised to verify the correlation is outlined in Fig. 1. Firstly, a uniform computational grid Ω having 500×500 points and centered at the target body is built over the square domain

---

[1]Values too small ($< 10^{-3}$) could generate false positives in the output binary image. The larger the final true anomaly, the larger is the threshold suggested to use. The trend is justified because changes in the LD value at the separatrices are stronger for longer propagations.
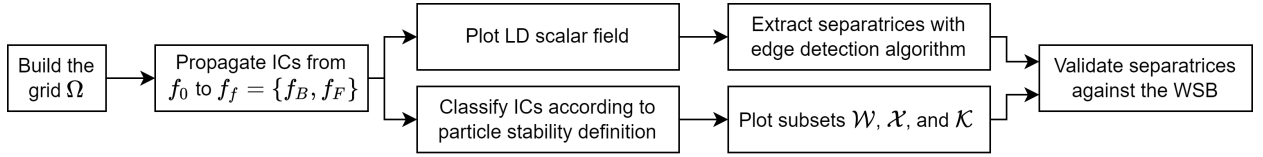
Figure 1: Validation workflow.

$[-\varepsilon, \varepsilon] \times [-\varepsilon, \varepsilon]$, with $\varepsilon = 6 \times 10^{-4}$. At f_0, the particle is assumed at the periapsis of an osculating prograde elliptic orbit about the target body with given eccentricity $e_0 = 0.9$ (see [19] for more details). Secondly, ICs are propagated in the $[f_0, f_f]$ interval. The LD values are computed and the ICs are allocated into the sets $\mathcal{W}$, $\mathcal{X}$, or $\mathcal{K}$ according to the stability definition discussed in Section 3.2. Then, the separatrices are extracted with the edge detection algorithm. Finally, the patterns are inspected against the WSB.
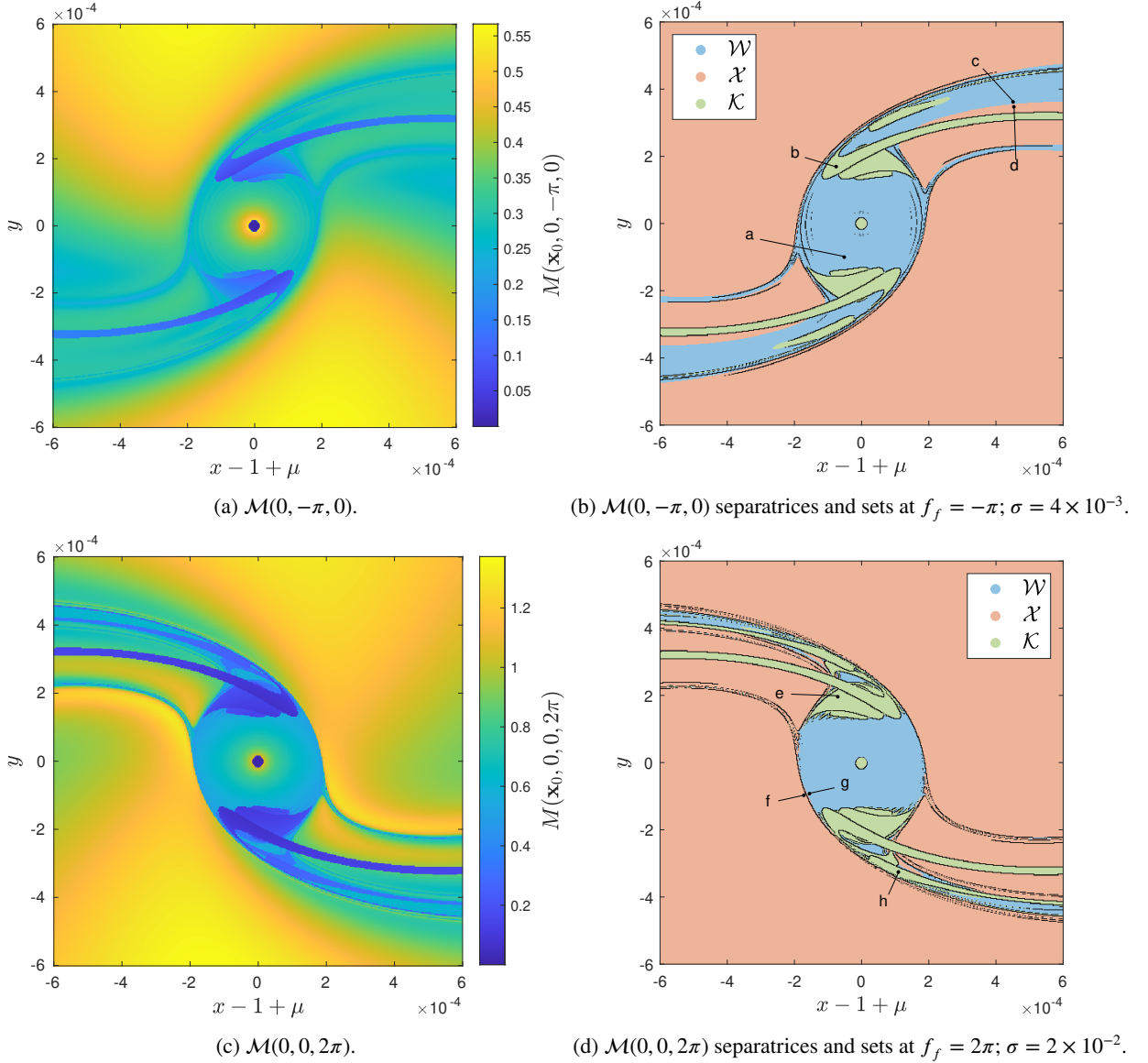
4. Results

Without loss of generality, the LD-based approach is applied to the Sun–Mars system. The correlation between the extracted separatrices and the WSB is tested for several integration intervals, for both forward and backward propagations. In Fig. 2, the LD scalar field computed for two distinct final anomalies is shown (see Figs. 2a and 2c), together with the extracted patterns overlapped to the subsets $\mathcal{W}$, $\mathcal{X}$, and $\mathcal{K}$ derived for the same f_f (see Figs. 2b and 2d). In both cases a good match between separatrices and boundaries of the classified regions is observed. The central green disk identifies ICs located inside the surface of Mars, which immediately generate crash orbits. The scalar field in Fig. 2c is more accurate in revealing the geometrical structures that characterize the ER3BP dynamics, when compared to that in Fig. 2a. The longer the finite horizon over which ICs are propagated, the more separatrices the field is able to reveal [20, 21, 24]. Since initial states in $\mathcal{M}(0, -\pi, 0)$ are integrated over a shorter finite horizon, the field cannot reveal structures with the same level of detail as compared with $\mathcal{M}(0, 0, 2\pi)$, in which initial states are propagated over a longer finite horizon. Results for the case $\mathcal{M}(0, -2\pi, 0)$, here not included, reach the same accuracy of the ones for the $\mathcal{M}(0, 0, 2\pi)$ field. Indeed, the two LD fields are symmetric with respect to the x-axis [16].

For small values of f_f, the matching presents some inconsistencies that are intrinsic to the LD definition. In fact, LD reveals patterns if ICs are integrated long enough for dynamical divergences between orbits to be manifested [24]. Consequently, the classification of the phase space according to the definition of particle stability provided in Section 3.2 may be inconsistent with some regions featured by the LD scalar field if the trajectories are not sufficiently divergent to feature singular structures in the field [24]. The latter is particularly true for short integration intervals as observed in Fig. 2b. For instance, ICs 'c' and 'd' in Fig. 2b are classified into two different sets, still their dynamical behavior is very similar as shown by their orbits in Figs. 4c and 4d. Indeed, for a slightly larger integration interval both orbits escape from Mars.

Remarkably, LDs detect divergence (forward propagation) and attraction (backward propagation) in the dynamical behavior even in areas classified in the same way according to our particle stability definition. To illustrate this concept, two grid points can evolve both in crash orbits, nonetheless their trajectories could be strongly different, as well as their impact epochs. For example, samples 'e' and 'h' in Fig. 2d belong to two distinct regions of the same crash set $\mathcal{K}(2\pi)$, therefore they both impact with Mars. However, they exhibit dissimilar trajectories (see Figs. 4e and 4h). They impact from different directions, and orbit 'h' reverses its angular momentum with respect to Mars much earlier than orbit 'e'.

Patterns ruling particles transport in both true anomaly directions are revealed combining the LD structures propagated forwards and backwards [24]. The correlation of the two capture sets $\mathcal{C}(-\pi, 3\pi/2)$ and $\mathcal{C}(-\pi, 3\pi)$ with the separatrices extracted from $\mathcal{M}(0, -\pi, 3\pi/2)$ and $\mathcal{M}(0, -\pi, 3\pi)$ fields, respectively, is presented in Fig. 3. Results show that some of the areas in the phase space enclosed by LD separatrices appear to be capture sets. Based on the outcome of the validation procedure, the devised methodology of computing the LD field and extracting the dynamics separatrices has been proven successful.

Referring to Fig. 3, the LD approach omits the dynamical behavior featured by the highlighted numerous regions, therefore a classification technique is still required to discern which areas are actually capture sets. A viable strategy to overcome the aforementioned limitation is proposed for practical design of BC orbits. By sampling an individual IC for each identified region and classifying its orbit, all areas in the phase space can be easily categorized either as $\mathcal{W}$, $\mathcal{X}$, or $\mathcal{K}$ subsets according to the particle stability definition given in Section 3.2.

(a) $\mathcal{M}(0, -\pi, 0)$.

(b) $\mathcal{M}(0, -\pi, 0)$ separatrices and sets at $f_f = -\pi$; $\sigma = 4 \times 10^{-3}$.

(c) $\mathcal{M}(0, 0, 2\pi)$.

(d) $\mathcal{M}(0, 0, 2\pi)$ separatrices and sets at $f_f = 2\pi$; $\sigma = 2 \times 10^{-2}$.

Figure 2: Validation of separatrices extracted from LD field through inspection against the WSB. Left: LD scalar field. Right: Extracted separatrices inspected against subsets $\mathcal{W}(f_f)$, $\mathcal{X}(f_f)$, and $\mathcal{K}(f_f)$.

The exact ICs sampled from Figs. 2 and 3 are collected in Table 2. Their orbits expressed in the Mars-centered, non-rotating frame, oriented as the synodic frame at f_0, and with Cartesian coordinates X and Y are plotted in Fig. 4. Compared to similar BC orbits found in the literature [19, 23], the weakly stable trajectories shown in Fig. 4 do not fully complete the last revolution about Mars due to the dropping of the usual geometrical constraint on the revolutions number. Nevertheless, they grant temporary capture at least over the finite horizon specified by the integration interval.

5. Conclusion

This study looks into the effectiveness of Lagrangian descriptors in revealing phase space organizing structures when facing the ballistic capture phenomenon, so investigating their capability in highlighting the weak stability boundary. They successfully reveal the geometrical structures governing the transport mechanisms that are then extracted through an edge detection algorithm based on the Roberts' operator to approximate the gradient of the
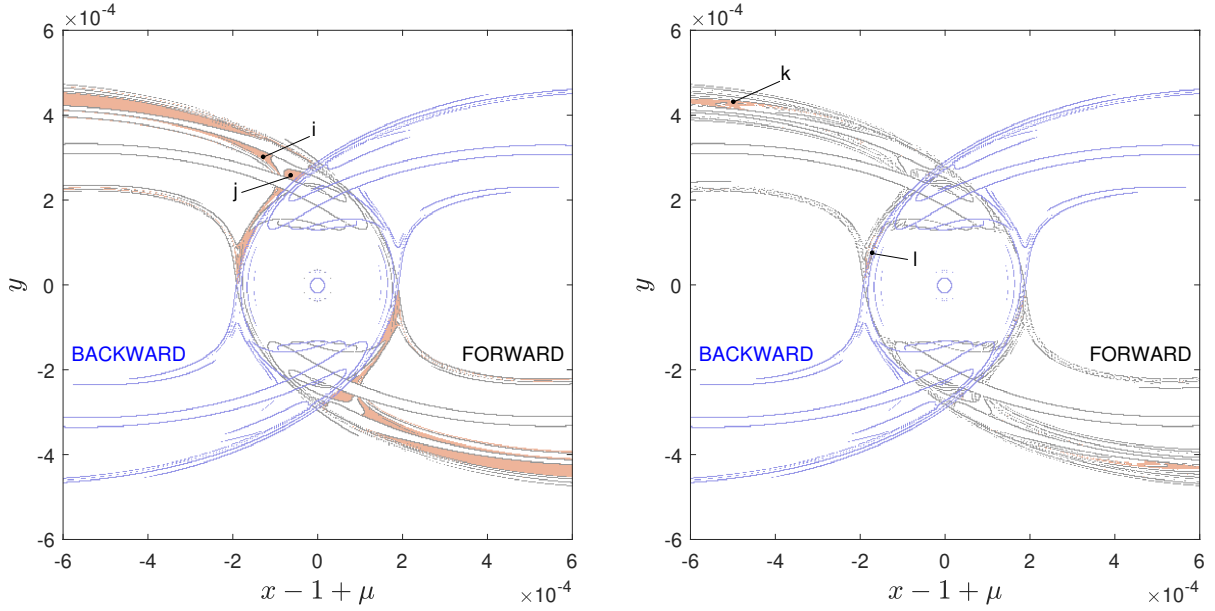
(a) $\mathcal{M}(0, -\pi, 3\pi/2)$ separatrices inspected against capture set $\mathcal{C}(-\pi, 3\pi/2)$. Sensitivity threshold σ set to 4×10^{-3} and 9×10^{-3} for backward and forward propagations, respectively.

(b) $\mathcal{M}(0, -\pi, 3\pi)$ separatrices inspected against capture set $\mathcal{C}(-\pi, 3\pi)$. Sensitivity threshold σ set to 4×10^{-3} and 3×10^{-2} for backward and forward propagations, respectively.
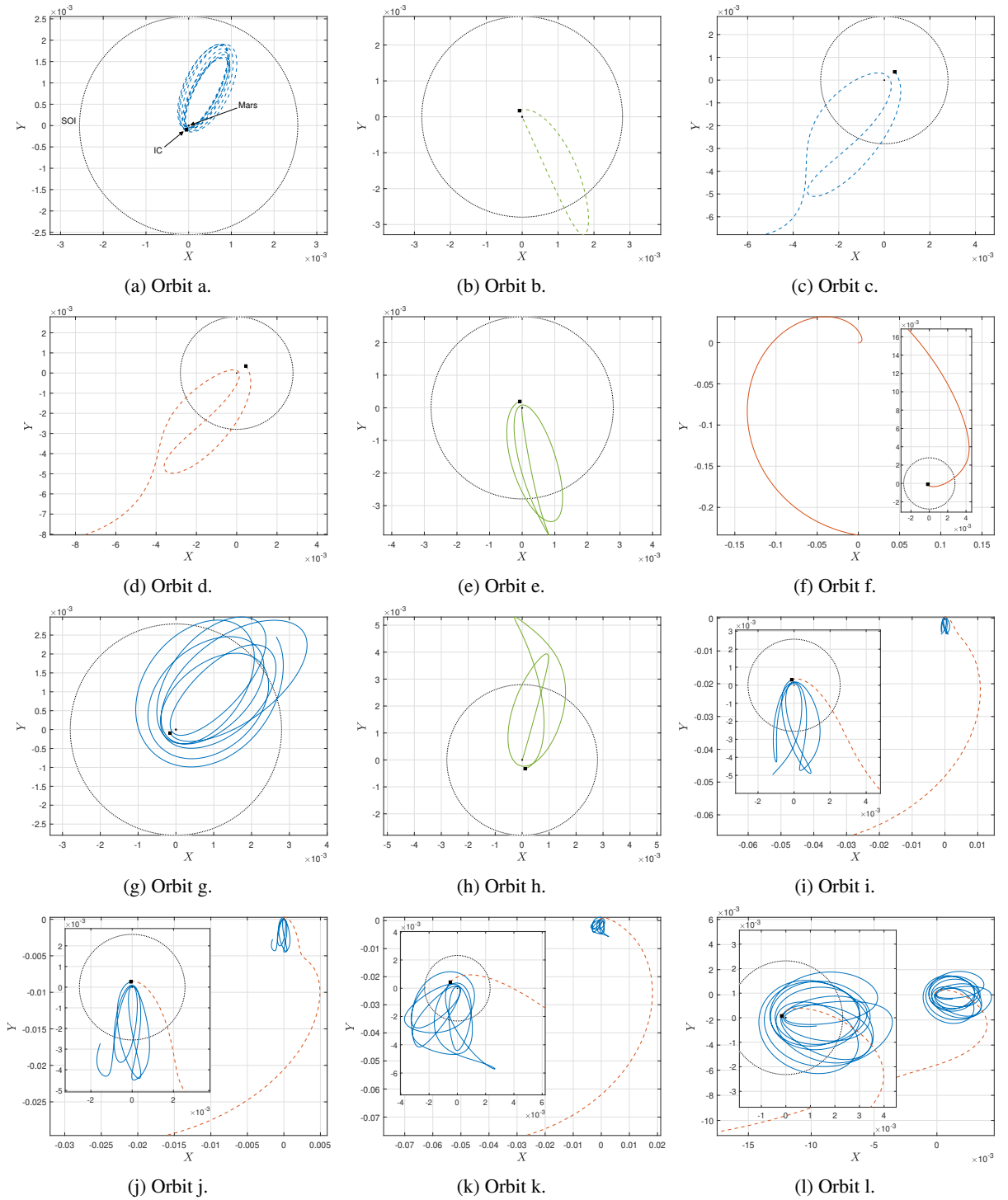
Figure 3: Inspection of separatrices extracted from $\mathcal{M}(0, f_B, f_F)$ against capture sets. Forward and backward separatrices of the LD field are represented as gray and blue lines, respectively.

Table 2
Initial conditions of sample orbits.

Orbit	Initial condition at $f_0 = 0$				Set
	$X_0 = x_0 - 1 + \mu$	$Y_0 = y_0$	x'_0	y'_0	
a	$-5.170\,000 \times 10^{-5}$	$-1.000\,000 \times 10^{-4}$	$6.258\,637 \times 10^{-2}$	$-3.235\,715 \times 10^{-2}$	$\mathcal{W}(-\pi)$
b	$-7.575\,000 \times 10^{-5}$	$1.695\,000 \times 10^{-4}$	$-4.999\,940 \times 10^{-2}$	$-2.234\,486 \times 10^{-2}$	$\mathcal{K}(-\pi)$
c	$4.509\,000 \times 10^{-4}$	$3.621\,000 \times 10^{-4}$	$-1.913\,330 \times 10^{-2}$	$2.382\,548 \times 10^{-2}$	$\mathcal{W}(-\pi)$
d	$4.533\,000 \times 10^{-4}$	$3.475\,000 \times 10^{-4}$	$-1.871\,302 \times 10^{-2}$	$2.441\,039 \times 10^{-2}$	$\mathcal{X}(-\pi)$
e	$-7.094\,000 \times 10^{-5}$	$1.960\,000 \times 10^{-4}$	$-4.856\,863 \times 10^{-2}$	$-1.757\,887 \times 10^{-2}$	$\mathcal{K}(2\pi)$
f	$-1.719\,000 \times 10^{-4}$	$-9.739\,000 \times 10^{-5}$	$2.616\,042 \times 10^{-2}$	$-4.617\,492 \times 10^{-2}$	$\mathcal{X}(2\pi)$
g	$-1.551\,000 \times 10^{-4}$	$-9.239\,000 \times 10^{-5}$	$2.842\,583 \times 10^{-2}$	$-4.771\,994 \times 10^{-2}$	$\mathcal{W}(2\pi)$
h	$1.094\,000 \times 10^{-4}$	$-3.258\,000 \times 10^{-4}$	$3.796\,152 \times 10^{-2}$	$1.274\,705 \times 10^{-2}$	$\mathcal{K}(2\pi)$
i	$-1.286\,000 \times 10^{-4}$	$3.018\,000 \times 10^{-4}$	$-3.772\,815 \times 10^{-2}$	$-1.607\,634 \times 10^{-2}$	$\mathcal{C}(-\pi, 3\pi/2)$
j	$-6.373\,000 \times 10^{-5}$	$2.585\,000 \times 10^{-4}$	$-4.429\,485 \times 10^{-2}$	$-1.092\,035 \times 10^{-2}$	$\mathcal{C}(-\pi, 3\pi/2)$
k	$-4.990\,000 \times 10^{-4}$	$4.317\,000 \times 10^{-4}$	$-1.863\,920 \times 10^{-2}$	$-2.154\,496 \times 10^{-2}$	$\mathcal{C}(-\pi, 3\pi)$
l	$-1.719\,000 \times 10^{-4}$	$7.575\,000 \times 10^{-5}$	$-2.195\,327 \times 10^{-2}$	$-4.981\,872 \times 10^{-2}$	$\mathcal{C}(-\pi, 3\pi)$

Lagrangian descriptor scalar fields. The extracted separatrices effectively distinguish regions with different dynamical behavior. The detected patterns are in good agreement with the weak stability boundary computed on the same integration interval. Lagrangian descriptors proved to be an intuitive, easy to implement, and convenient tool for designing ballistic capture orbits. Without any a priory knowledge, Lagrangian descriptor patterns yield a consistent match with the weak stability boundary and the associated stable sets. The proposed methodology supports the design of ballistic capture orbits, enriching the dynamics knowledge in the proximity of the target planet. Furthermore, the technique can be successfully applied to arbitrary non-autonomous, more representative, astrodynamics models without any restrictions.

(a) Orbit a.

(b) Orbit b.

(c) Orbit c.

(d) Orbit d.

(e) Orbit e.

(f) Orbit f.

(g) Orbit g.

(h) Orbit h.

(i) Orbit i.

(j) Orbit j.

(k) Orbit k.

(l) Orbit l.

Figure 4: Sample orbits in the Mars-centered, non-rotating frame. Forward ($f > f_0$) and backward ($f < f_0$) legs plotted as solid and dashed lines, respectively; Mars' SOI represented as a black dotted circumference. ICs indicated with square markers. Coloring identifies the subset the orbits belong to, according to the color code used in Fig. 2. ICs collected in Table 2.

CRediT authorship contribution statement

Declaration of competing interest

The authors declare that they have no known competing financial interests or personal relationships that could have appeared to influence the work reported in this paper.

Acknowledgment

References

[1] Belbruno, E., 1987. Lunar capture orbits, a method of constructing Earth Moon trajectories and the lunar GAS mission, in: 19th International Electric Propulsion Conference, American Institute of Aeronautics and Astronautics. pp. 1–9. doi:10.2514/6.1987-1054.

[2] Belbruno, E., 2004. Capture Dynamics and Chaotic Motions in Celestial Mechanics. Princeton University Press. doi:10.1515/9780691186436.

[3] Belbruno, E., Carrico, J., 2000. Calculation of weak stability boundary ballistic lunar transfer trajectories, in: Astrodynamics Specialist Conference, pp. 4142, 262–271. doi:10.2514/6.2000-4142.

[4] Belbruno, E., Gidea, M., Topputo, F., 2010. Weak stability boundary and invariant manifolds. SIAM Journal on Applied Dynamical Systems 9, 1061–1089. doi:10.1137/090780638.

[5] Belbruno, E., Miller, J., 1990. A ballistic lunar capture trajectory for the Japanese spacecraft Hiten. Technical Report. Jet Propulsion Laboratory. IOM 312/90.4-1731-EAB.

[6] Belbruno, E., Miller, J., 1993. Sun-perturbed Earth-to-Moon transfers with ballistic capture. Journal of Guidance, Control, and Dynamics 16, 770–775. doi:10.2514/3.21079.

[7] Bernardini, N., Merisio, G., Losacco, M., Raffa, S., Armellin, R., Baresi, N., Lizy-Destrez, S., Topputo, F., Canalias, E., et al., 2022. Exploiting coherent patterns for the analysis of qualitative motion and the design of bounded orbits around small bodies, in: 73rd International Astronautical Congress (IAC 2022), pp. 1–16.

[8] Caleb, T., Merisio, G., Di Lizia, P., Topputo, F., 2022. Stable sets mapping with Taylor differential algebra with application to ballistic capture orbits around Mars. Celestial Mechanics and Dynamical Astronomy 134, 39. doi:10.1007/s10569-022-10090-8.

[9] Campagnola, S., Russell, R.P., 2010. Endgame problem part 2: Multibody technique and the Tisserand-Poincare graph. Journal of Guidance, Control, and Dynamics 33, 476–486. doi:10.2514/1.44290.

[10] Carletta, S., Pontani, M., Teofilatto, P., 2019. Design of low-energy capture trajectories in the elliptic restricted four-body problem, in: 70th International Astronautical Congress (IAC 2019), pp. 21–25.

[11] Circi, C., Teofilatto, P., 2001. On the dynamics of weak stability boundary lunar transfers. Celestial Mechanics and Dynamical Astronomy 79, 41–72. doi:10.1023/A:1011153610564.

[12] Conley, C.C., 1968. Low energy transit orbits in the restricted three-body problems. SIAM Journal on Applied Mathematics 16, 732–746. doi:10.1137/0116060.

[13] Conley, C.C., 1969. On the ultimate behavior of orbits with respect to an unstable critical point I. Oscillating, asymptotic, and capture orbits. Journal of Differential Equations 5, 136–158. doi:10.1016/0022-0396(69)90108-9.

[14] Davis, L.S., 1975. A survey of edge detection techniques. Computer Graphics and Image Processing 4, 248–270. doi:10.1016/0146-664X(75)90012-X.

[15] García, F., Gómez, G., 2007. A note on weak stability boundaries. Celestial Mechanics and Dynamical Astronomy 97, 87–100. doi:10.1007/s10569-006-9053-6.

[16] Gawlik, E.S., Marsden, J.E., Du Toit, P.C., Campagnola, S., 2009. Lagrangian coherent structures in the planar elliptic restricted three-body problem. Celestial Mechanics and Dynamical Astronomy 103, 227–249.

[17] Haller, G., 2011. A variational theory of hyperbolic Lagrangian coherent structures. Physica D: Nonlinear Phenomena 240, 574–598. doi:10.1016/j.physd.2010.11.010.

[18] Haller, G., 2015. Lagrangian coherent structures. Annual Review of Fluid Mechanics 47, 137–162. doi:10.1146/annurev-fluid-010313-141322.

[19] Hyeraci, N., Topputo, F., 2010. Method to design ballistic capture in the elliptic restricted three-body problem. Journal of Guidance, Control, and Dynamics 33, 1814–1823. doi:10.2514/1.49263.

[20] Jiménez Madrid, J.A., Mancho, A.M., 2009. Distinguished trajectories in time dependent vector fields. Chaos: An Interdisciplinary Journal of Nonlinear Science 19, 013111, 1–19. doi:10.1063/1.3056050.

[21] Lopesino, C., Balibrea-Iniesta, F., García-Garrido, V.J., Wiggins, S., Mancho, A.M., 2017. A theoretical framework for Lagrangian descriptors. International Journal of Bifurcation and Chaos 27, 1730001, 1–25. doi:10.1142/s0218127417300014.

[22] Luo, Z.-F., Topputo, F., 2015. Analysis of ballistic capture in Sun–planet models. Advances in Space Research 56, 1030–1041. doi:10.1016/j.asr.2015.05.042.

[23] Luo, Z.-F., Topputo, F., Bernelli-Zazzera, F., Tang, G.-J., 2014. Constructing ballistic capture orbits in the real solar system model. Celestial Mechanics and Dynamical Astronomy 120, 433–450. doi:10.1007/s10569-014-9580-5.

[24] Mancho, A.M., Wiggins, S., Curbelo, J., Mendoza, C., 2013. Lagrangian descriptors: A method for revealing phase space structures of general time dependent dynamical systems. Communications in Nonlinear Science and Numerical Simulation 18, 3530–3557. doi:10.1016/j.cnsns.2013.05.002.

[25] Manzi, M., Topputo, F., 2021. A flow-informed strategy for ballistic capture orbit generation. Celestial Mechanics and Dynamical Astronomy 133, 1–16. doi:10.1007/s10569-021-10048-2.

[26] Merisio, G., 2023. Engineering ballistic capture for autonomous interplanetary spacecraft with limited onboard resources (PhD Thesis). Politecnico di Milano, Milan, Italy. URL: http://hdl.handle.net/10589/196152.

[27] Montenbruck, O., Gill, E., 2000. Satellite Orbits Models, Methods and Applications. Springer. doi:10.1007/978-3-642-58351-3.

[28] Raffa, S., Merisio, G., Topputo, F., 2023. Finding regions of bounded motion in binary asteroid environment using Lagrangian descriptors. Communications in Nonlinear Science and Numerical Simulation , 107198doi:10.1016/j.cnsns.2023.107198.

[29] Restrepo, R.L., Russell, R.P., 2017. Patched periodic orbits: A systematic strategy for low energy transfer design, in: AAS/AIAA Astrodynamics Specialist Conference, pp. 17–695.

[30] Roberts, L.G., 1963. Machine perception of three-dimensional solids (PhD Thesis). Massachusetts Institute of Technology.

[31] Sousa Silva, P., Terra, M., 2012. Applicability and dynamical characterization of the associated sets of the algorithmic weak stability boundary in the lunar sphere of influence. Celestial Mechanics and Dynamical Astronomy 113, 141–168. doi:10.1007/s10569-012-9409-z.

[32] Topputo, F., Belbruno, E., 2009. Computation of weak stability boundaries: Sun–Jupiter system. Celestial Mechanics and Dynamical Astronomy 105, 3–17. doi:10.1007/s10569-009-9222-5.

[33] Topputo, F., Belbruno, E., 2015. Earth–Mars transfers with ballistic capture. Celestial Mechanics and Dynamical Astronomy 121, 329–346. doi:10.1007/s10569-015-9605-8.

[34] Topputo, F., Vasile, M., Bernelli-Zazzera, F., 2005. Low energy interplanetary transfers exploiting invariant manifolds of the restricted three-body problem. The Journal of the Astronautical Sciences 53, 353–372. doi:10.1007/BF03546358.

[35] Tyler, J., Wittig, A., 2022. An improved numerical method for hyperbolic Lagrangian coherent structures using differential algebra. Journal of Computational Science 65, 101883. doi:10.1016/j.jocs.2022.101883.

[36] Verner, J.H., 2010. Numerically optimal Runge–Kutta pairs with interpolants. Numerical Algorithms 53, 383–396. doi:10.1007/s11075-009-9290-3.

[37] Wittig, A., Di Lizia, P., Armellin, R., Makino, K., Bernelli-Zazzera, F., Berz, M., 2015. Propagation of large uncertainty sets in orbital dynamics by automatic domain splitting. Celestial Mechanics and Dynamical Astronomy 122, 239–261. doi:10.1007/s10569-015-9618-3.